Monthly Notices
of the
ROYAL ASTRONOMICAL SOCIETY

MNRAS **455,** 343–356 (2016) doi:10.1093/mnras/stv2080

On the estimation of a celestial reference frame in the presence of source structure

L. Plank,[1]★ S. S. Shabala,[1] J. N. McCallum,[1] H. Krásná,[2] B. Petrachenko,[3] E. Rastorgueva-Foi[1] and J. E. J. Lovell[1]

[1]*University of Tasmania, School of Physical Sciences, Private Bag 37, Hobart, 7001, Australia*
[2]*Technische Universität Wien, Department of Geodesy and Geoinformation, Gußhausstraße 27–29, Vienna, 1040, Austria*
[3]*Natural Resources Canada, Canadian Geodetic Survey, 588 Booth St, Ottawa, Canada*

Accepted 2015 September 7. Received 2015 June 29; in original form 2015 March 28

ABSTRACT

The spatial structure of sources making up the celestial reference frame (CRF) at radio frequencies is a systematic error source in very long baseline interferometry (VLBI) measurements. Using simulations, we investigate the effects of source structure on the CRF, determined by the actual observational programme of the International VLBI Service for Geodesy and Astrometry. This is done using the source structure simulator of the Vienna VLBI Software. Applying various mock two-component source models, systematic displacements of 10–80 μas in median source position offsets are found. These offsets are predominantly aligned with the direction of the jet. The simulations further show that slight changes in the source model can significantly change the estimated positions. We finally present a new parametrization of source positions in the analysis, namely along the jet direction and perpendicular to it, allowing us to significantly mitigate the effects of source structure on an estimated CRF.

Key words: techniques: interferometric – astrometry – reference systems – quasars: general.

1 INTRODUCTION

Very long baseline interferometry (VLBI) positions of extragalactic radio sources (quasars) realize the International Celestial Reference Frame (ICRF2; Ma et al. 2009) at radio frequencies. As the fundamental inertial celestial reference frame, the ICRF2 is widely used in astrometry, spacecraft navigation and geodesy. Originally chosen on the hypothesis that the measured extragalactic radio sources are at rest and point sources, at current accuracies this assumption is no longer acceptable. Most observed sources exhibit spatially extended structures that are variable in both time and frequency. The structure and kinematics of compact extragalactic radio sources have been the subject of astrophysical studies since their discovery more than four decades ago (Cohen et al. 1971; Knight et al. 1971; Whitney et al. 1971). Currently, some geodetic sources have a long history of structure evolution monitoring with high spatial resolution (e.g. Piner et al. 2007; Lister et al. 2009; Homan 2012; Ros 2012; Lister et al. 2013), and their effect on geodetic measurements has long been recognized (Charlot 1990). A direct correction of the effects for geodetic and astrometric VLBI requires detailed knowledge of the sources' inner structures, as obtained for example by regular source imaging (Charlot 1990). In several studies (e.g. Charlot 1993; Sovers et al. 2002; Tornatore & Charlot 2007), source corrections have been applied in VLBI analysis. Despite showing minor improvements and proving the existence of source structure effects in geodetic VLBI data, these studies also clearly revealed the difficulties in making structure corrections. As structure varies with time (e.g. Lister et al. 2009; Shabala et al. 2014), having reliable and up-to-date source maps is one issue. In addition, for many sources, the effects are small and an order of magnitude below the currently dominating errors due to tropospheric delays (e.g. Shabala et al. 2015).

The common present-day solution to the source structure problem is a careful selection of suitable sources that presumably only show minor structure, according to a specifically defined source structure index (SI) <3.0 (Ma et al. 2009). The SI was introduced by Fey & Charlot (1997) and modified to a continuous scale in Ma et al. (2009). Calculated as

$$\mathrm{SI} = 1 + 2\log(\tau_{\mathrm{median}}), \quad (1)$$

it indicates the expected magnitude of delays due to source structure on VLBI measurements. Hereby, τ_{median} (in picosec) is the median of all structure delays calculated for all projected baselines possible for Earth-bound VLBI. While this might be an appropriate solution now, in the future new mitigation strategies will have to be found. As pointed out by Porcas (2009, 2010), future accuracy demands, along with a major change in the VLBI observing strategy (VGOS; Petrachenko et al. 2009), as well as new astrometric challenges, such as the alignment of the ICRF radio frame to the

★ E-mail: Lucia.Plank@utas.edu.au

future GAIA frame at optical frequencies (Lindegren et al. 2008), will require a more careful treatment of source structure effects. Besides contributing to the overall error budget of VLBI measurements as a systematic delay depending on the relative orientation of the source and the VLBI baseline (e.g. Sovers, Fanselow & Jacobs 1998), a temporal change in the brightness distribution of a source might also result in an apparent motion of this source (Ma et al. 1998). Fey & Charlot (1997) showed that the size of the source structure (as, for example, determined by the SI) correlates with both the ICRF position accuracy and also with the magnitude of observed time variations in the source coordinates. Schaap et al. (2013) confirmed the relation between observed source position uncertainties and structure indices, and further could relate greater position stability to the astrophysical property of scintillation. Charlot (1993) and Sovers et al. (2002) found a decrease in position variability for certain sources when structure corrections were applied in VLBI analysis. A different concept was chosen by MacMillan & Ma (2007) who suggested modelling the positions of unstable sources as arc parameters (i.e. essentially unconstrained values determined on a session-by-session basis) rather than global positions over all sessions. A similar concept is chosen in Section 4.

The measured emission at radio frequencies of geodetic quasars arises from highly relativistic jets, which lie at angles close to our line of sight. Structure evolution in terms of outbursts of the core usually occur along the jet direction, which itself is quite stable with time (Lister et al. 2009). In a statistical analysis, Moór et al. (2009) found a general correlation between the direction of the observed proper motion of a source and the characteristic direction of the jet.

The goal of this paper is to use simulations to investigate whether in an estimated CRF of standard geodetic VLBI observations, the effects of source structure can move sources along the jet direction. Here, a movement of a source means the estimated source position, as determined through a set of VLBI sessions. In this contribution, we determine the magnitude and characteristics of this displacement for a suite of mock two-component models with different structure indices. We do not simulate quasar variability. We then implement a new parametrization for the estimation of a CRF, with the goal to mitigate these effects. The strategy applied is that the common parametrization into right ascension (RA) and declination (Dec.) is converted into a component parallel (j) to the jet direction of each source and one perpendicular (n) to it. As we expect the source to be unstable predominantly in the j-direction, this component is estimated as an arc parameter for each session, while the normal component is estimated as a global parameter contributing to the CRF. All our investigations in this paper are performed using simulations and mock models of source structure.

First, we introduce our simulation method in Section 2, providing information on the VLBI schedules used, the source structure simulator and our strategy to estimate a celestial reference frame. In Section 3, we investigate the effects of source structure on a globally estimated CRF. We present results of different simulations, and use various structure models of different structure indices. We present a new parametrization for the mitigation of source structure effects in Section 4 and we discuss the results of this analysis in Section 5. We conclude in Section 6.

2 SIMULATION METHOD

We use the schedules of one year of standard geodetic VLBI sessions, the 2013 rapid turnaround sessions (R1, R4) of the International VLBI Service for Geodesy and Astrometry (IVS; Schuh & Behrend 2012). These R-sessions are undertaken twice a week for 24 h, using a global antenna network of 7–11 stations that can change from one session to the next (e.g. Plank et al. 2015). Because of their regularity and timeliness in correlation and analysis, these sessions constitute the majority of the IVS data and heavily contribute to its main products: the terrestrial reference frame, the Earth orientation parameters and the CRF. The Vienna VLBI Software (VieVS; Böhm et al. 2012) allows us to simulate and analyse these observations. In geodetic/astrometric analysis (e.g. Sovers et al. 1998; Schuh & Böhm 2013), the group delay τ is the main observable, defined as the difference in signal arrival time at the two antennas of a baseline. This delay is determined in the correlation process, as a combination of the measurements recorded in multiple frequency channels. In the analysis, the observable (O) is approximated with the computed delay (C). This is done using best possible a priori information for station and source coordinates, Earth orientation and relativistic effects, as well as models for various geophysically induced station movements, media delays and antenna instrumental delays. The residuals (O − C) enter the estimation part (e.g. least-squares adjustment), allowing us to estimate corrections to the a priori values (e.g. improved source positions).

In a subsequent global solution (Krásná et al. 2014), the normal equation matrices of all individual 24-h sessions are combined, determining global source positions as a single common solution of all sessions. Although for a real determination of the CRF data one year is usually not sufficient, it is enough for the purposes of our investigations. The limiting factor here is simply the computing time it takes to perform simulations using the various source models.

2.1 Source models

In order to simulate the effects of source structure, we created mock catalogues (Table 1), assigning to all sources a nominal SI (Ma et al. 2009) of SI = 2, 3 or 4. The sources were modelled having two components, with the second component having a relative brightness b_r and separation s (in mas) from the main component. The direction of the jet, corresponding to the direction between the two components of the source, was assigned randomly between 0° and 360° over all sources. For each of the eight X-band frequencies that are usually observed in geodetic VLBI, the additional phase term due to source structure can be calculated. This is done using the projection of the baseline in the source direction (e.g. Fey & Charlot 1997; Charlot 1990), on to the (u, v) plane. A fitted slope over all frequencies finally yields the additional group delay due to source structure (as described in Shabala et al. 2015). Source structure in the S-band was not taken into account in our study. S-band data are only used as an auxiliary band in geodetic VLBI and, despite a generally higher structural delay, the effects are highly diluted and are usually ignored (e.g. Porcas 2010).

This formalism was implemented in the source structure simulator of the geodetic analysis software VieVS. As described in Shabala et al. (2015), the simulator enables us to add a structure delay to the geodetic observable and to quantify its effects in the analysis.

Simple two-component models have traditionally been used in source structure studies, allowing for an analytical treatment of the additional delay (Charlot 1990). In our software, we use a numerical calculation that has been validated against the analytical formula of Charlot (1990). In principle, this allows for the usage of multicomponent models, as they can be derived from real images. For simplicity and a systematic comparison of various models, we chose to use two-component source models for our investigation. This representation is appropriate, as shown by a comparison with

Table 1. Source structure models used in the simulation. We use two-component sources described by two parameters: the relative brightness b_r of the second component to the main component and their separation s. In the third column, the distance of the centroid position from the main component r_{centr} (equation 2) is calculated. We also give the nominal median delay due to source structure τ_{nom} and its structure index (SI_{nom}; Ma et al. 2009) for all Earth-bound baselines. The last two columns give the actual median delay τ_{obs}, as measured in the simulated observations, and the respective delay index SI_{obs}.

b_r	s (mas)	r_{centr} (μas)	SI_{nom}	τ_{nom} (ps)	SI_{obs}	τ_{obs} (ps)
0.35	0.26	67	2.0	3.1	1.7	2.2
0.30	0.35	81	2.0	3.1	1.7	2.3
0.25	0.51	102	2.0	3.3	1.7	2.3
0.20	0.53	88	2.0	3.2	1.5	1.8
0.15	0.57	74	2.0	3.1	1.3	1.4
0.10	0.67	61	2.0	3.2	1.0	1.0
0.05	1.52	72	2.0	3.1	1.5	1.8
0.35	0.67	197	3.0	10.1	2.1	3.6
0.30	0.70	162	3.0	10.1	2.0	3.1
0.25	0.82	164	3.0	9.0	1.9	2.7
0.20	1.01	168	3.0	9.9	1.7	2.1
0.15	1.49	194	3.0	10.0	2.4	5.0
0.10	2.45	223	3.0	10.0	2.5	5.7
0.05	5.67	270	3.0	9.5	2.5	5.4
0.35	2.45	635	4.0	31.2	3.7	21.5
0.30	2.75	635	4.0	31.9	3.6	20.0
0.25	3.08	616	4.0	31.4	3.4	16.6
0.20	3.93	655	4.0	31.6	3.4	15.1
0.15	6.35	828	4.0	32.0	3.5	17.1

real source images from the Astrogeo[1] data base: for 50 per cent of the 103 frequently observed sources (see Section 2.2), we find only negligible residuals (<1 per cent of the peak amplitude) when fitting a two-component source model to the image. Using the same source images and restricting them to sources of SI = 2 and above, we find a median relative brightness b_r of 0.1 (with a maximum of 0.3) and a median offset s of 1.3 mas (with a maximum of 5–6 mas). Hence, the ranges of our source models were chosen accordingly.

Following equation (1), the median structure delay for all Earth-bound baselines defines a nominal SI (Ma et al. 2009). Hence, the chosen SI (SI_{nom}) of 2, 3 and 4 correspond to median structure delays of 3, 10 and 30 ps, respectively. In Fig. 1, the relation between the relative brightness of the second component and the separation between the two components is shown for nominal structure indices of 2, 3 and 4. In general, we see that more extended sources have a higher SI. Further, it is clear that a strong secondary component close by can have the same SI as a weak component further away. As additional information on the source models, the distance of the brightness centroid of the radio emission from the main component,

$$r_{centr} = \frac{b_r}{1 + b_r} s, \qquad (2)$$

is given in the third column of Table 1. By varying for the different models, we find the brightness centroid to be offset from the core (defined as the location of the main component) at the level of 60–100 μas for the SI = 2 models, 160–270 μas for the SI = 3 models and 600–830 μas for the SI = 4 models. Bouffet, Charlot & Lambert (2013) used observed changes in this brightness centroid as an indicator for varying sources and – to a certain extent – found a positive correlation between structural variations and measured source position instabilities.

[1] http://astrogeo.org

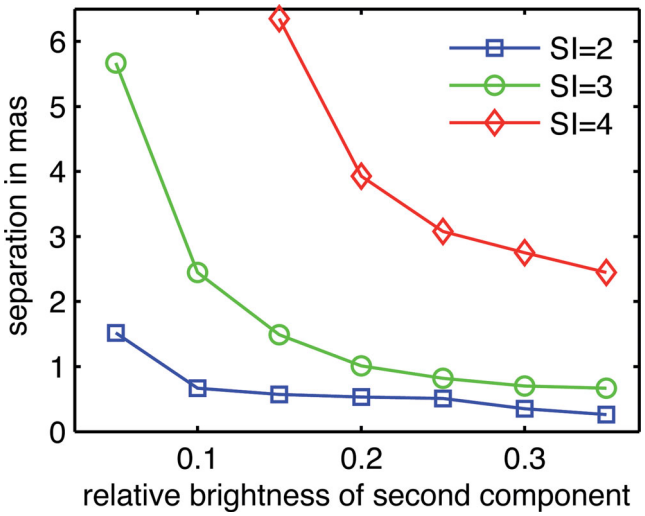

Figure 1. Relation between the relative brightness and the separation of the second component for nominal structure indices of SI = 2, 3 and 4. The values are those of Table 1.

More details on the various source models are given in Figs 2–4. In the left panel, the *X*-band delay (in ps) due to source structure is shown as a function of observing projected baseline in the direction of the source – the (u, v) plane – for all possible projected Earth-bound baselines. One baseline and observation combination is represented by a sample point in this graph. Longest baselines (up to the Earth's diameter) are on the edge of the circle while shorter baselines are represented in the middle of the circle. For illustration, the direction of the source extension (i.e. the line between the two components of the source) was chosen identically for all source models. Each baseline along the vertical axis has zero structure delay. When the structure group delay is plotted on the (u, v) plane, a clear pattern is apparent. The magnitude of the structure delay increases with both the relative strength of the secondary component and the baseline length in the direction of the source extension. The appearance of the delay is thus of stripes orthogonal to the source extension, with an opposite sign for each side of the (u, v) plane. The spatial frequency of the delay variations are inversely proportional to the angular separation of the secondary component.

In the second column of Figs 2–4, the distribution of the absolute structure delay is shown, from zero to 100 per cent of sampled baselines. The black thin line shows the distribution of evenly sampled baselines, used for the calculation of the nominal SI. The blue (thick) lines show the actual samples of structure delays for the projected baselines, as they were observed in the simulated sessions. For the latter, all sources were given the same structure model. As real VLBI networks do not cover the whole globe, the observed structure delays are generally smaller than the nominal ones. The median values (τ_{obs}) of this sampling for the various source models are given in the seventh column of Table 1. The corresponding observed SI (delay index SI_{obs}) is given in column 6.

When calculating the median structure delays for the observations in our simulation, we generally find much lower values than the nominal SI. This is due to the fact that longer baselines are generally more affected by source structure and that in our observed network the baselines are shorter than in the optimal network over all Earth

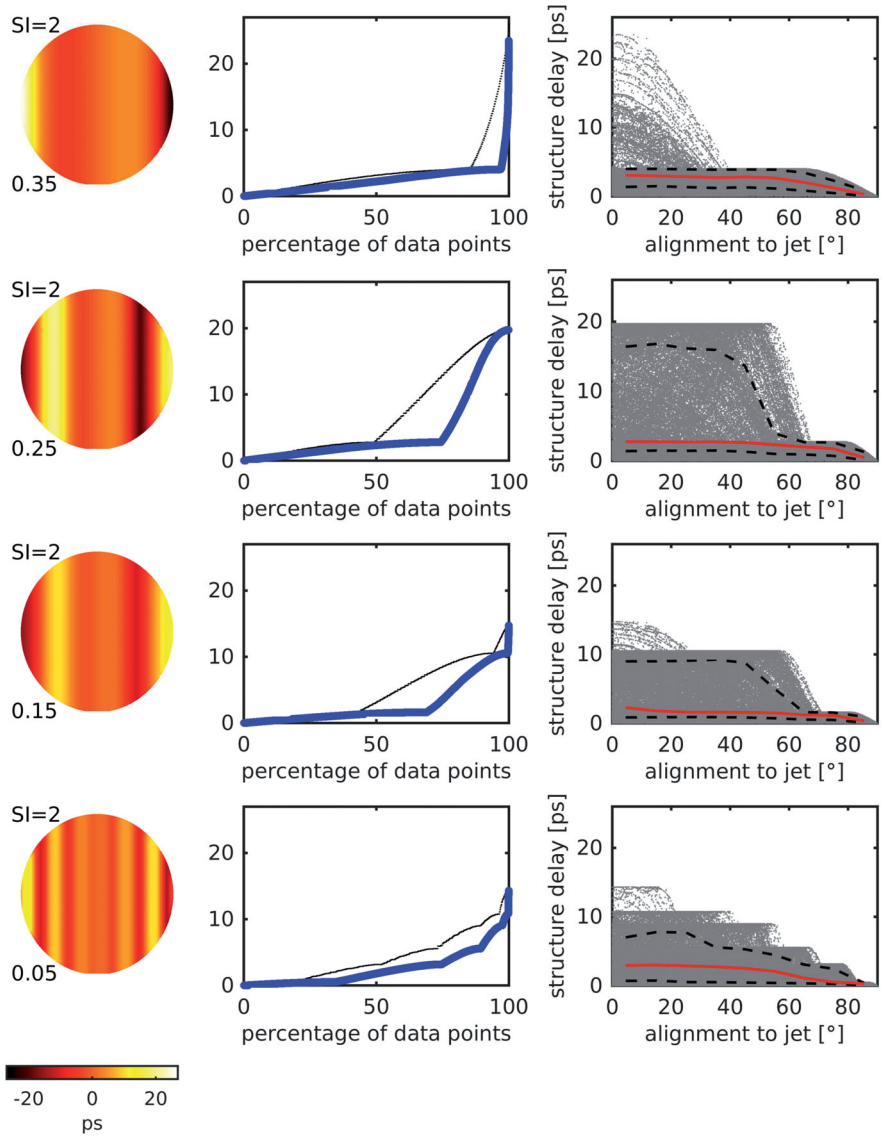

Figure 2. Source structure models for SI = 2. In the left panel, the *X*-band delay due to source structure in picoseconds is shown as a function of observing the projected baseline in the direction of the source. One baseline and observation is represented by one point in this graph, with longest baselines up to the Earth's diameter at the edge of the circle. The colour bar is identical for models of one SI. The middle panels show the distribution of the magnitude of structure delays in per cent, in black (thin) line for the nominal sampling over all Earth-bound baselines and in blue (thick) line for the sampling of the simulated observations. All simulated sources were given the identical source model. In the right panel, the observed structure delays are shown as a function of the alignment between the projected baseline and the jet direction of the source, with 0° corresponding to a projected baseline that is parallel to the jet direction, and 90° when this is orthogonal. Each grey point represents one observation. The values are then binned to steps of 10° in alignment angle, with the red solid line showing the median delays and the black dashed lines indicating the 1σ probability (16th and 84th percentiles). Each row represents one source model, with varying brightness ratios $b_r = 0.35$–0.05.

bound baselines that is used to calculate the nominal SI. In addition, the observed structure indices vary between the various models.

Studying the sampling curves (middle plots), we find that they are quite flat for the first half of the delays and then rise steeply at the end. For a stronger secondary component, this incline starts earlier than for a weaker secondary component. For the nominal global sampling, this hardly influences the median delays (50 per cent), with rather stable nominal delays of 3 ps, 10 ps, and 30 ps for SI = 2, SI = 3, and SI = 4 respectively, over all models. In real sampling, a different distribution of the delays explains the variation of the delay indices that is found amongst the source models of identical nominal SI (cf. Table 1). We also find that a source of a nominal SI of 2 (SI = 2, b_r = 0.25/0.30/0.35) can have the same delay index ($SI_{obs} = 1.7$) as a source of a nominal SI of 3 (SI = 3, b_r = 0.2). Clear differences in the observed delays between the various source models of one SI are further visible in the magnitude of the largest delays (10–25 ps for SI = 2, 25–50 ps for SI = 3 and 70–160 ps for SI = 4) as well as in the distribution of the upper 16 per cent of structure delays (84th percentile) versus the alignment to the direction of the jet. This is shown in the last column of Figs 2–4. It is also clearly visible that, as expected, the structure delay is generally higher when the baseline is aligned with the jet direction and zero when it is strictly perpendicular to it.

Overall, this investigation gives evidence for the complex interaction of source model, baseline length and observing geometry on the actual effective structure delay. It further shows that the value

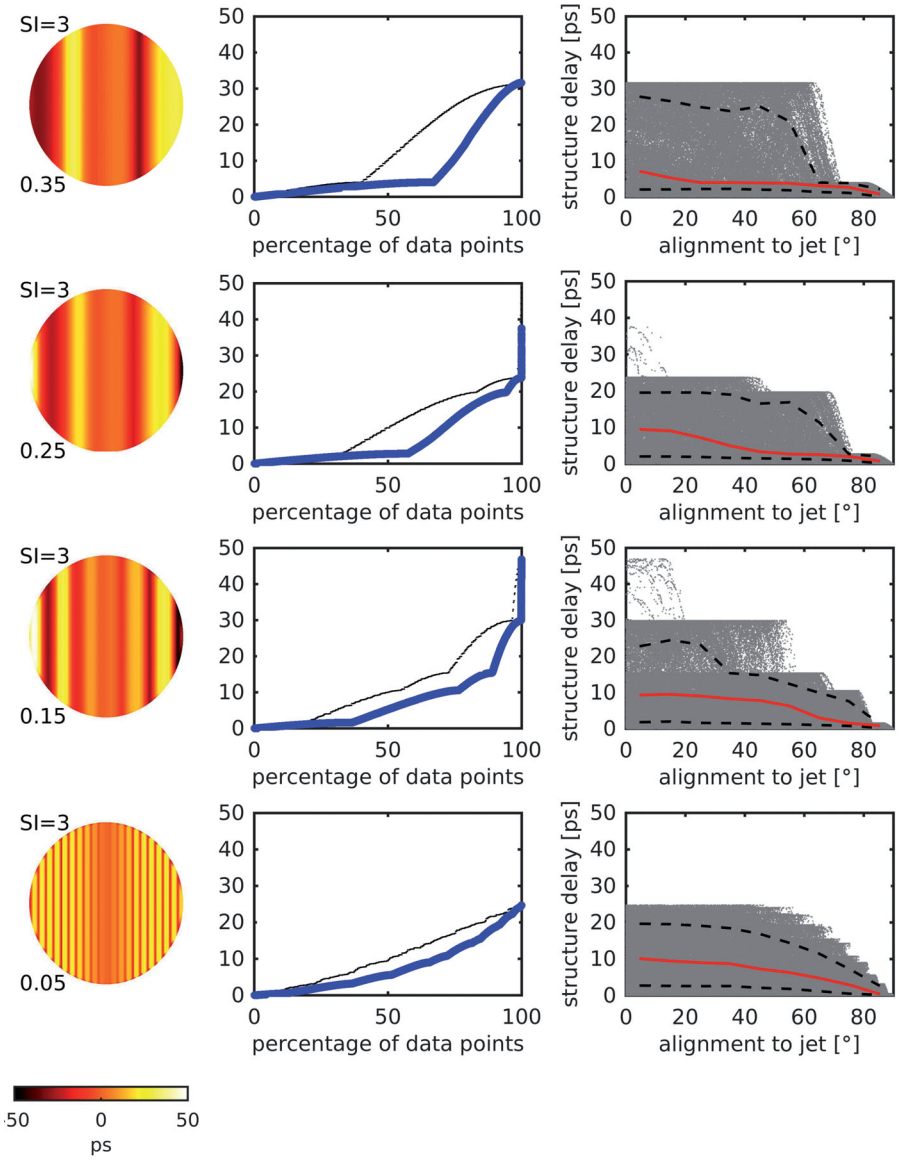

Figure 3. Same as Fig. 2, but for SI = 3.

of the nominal structure index SI_{nom} might not always adequately mirror the actual effects of structure delays for real observations performed with a specific observing network. For our investigated observations with global baselines, we find the nominal SI to be too high compared to the index as calculated with the actual baselines. The specific numbers in units of SI are 0.3–1.0 too high for the SI = 2 models, 0.5–1.3 for the SI = 3 models and 0.3–0.6 for the SI = 4 models. The fact that this offset is less for the SI = 4 models is a result of the higher beating of the structure delay pattern in the (u, v) plane (left panels of Fig. 4), which makes the sampling less susceptible to the actual observed baselines.

2.2 Simulation and processing

In the VieVS simulator, we can produce so-called zero-input observations, where we set the observations (O) equal to the values of the theoretical delay (C) as calculated in the analysis. In a second run, we can then add the effect of source structure τ_{ss}, allowing us to solely investigate its contribution to estimated geodetic products such as source positions. We call these source structure-only simulations. Alternatively, VieVS also allows us to simulate the effects of the most important stochastic error sources in geodetic VLBI, namely effects due to tropospheric turbulence τ_{trop}, station clocks τ_{clk} and measurement noise modelled as white noise per baseline τ_{wn}. More information on the simulation method can be found in Petrachenko et al. (2009) or Pany et al. (2011). The characteristic numbers (Nilsson, Haas & Elgered 2007) for the simulation of the turbulent troposphere were assumed to be identical at all stations with a structure constant $C_n = 1.5 \times 10^{-7}$ m$^{-1/3}$ over an effective height $H = 2000$ m, a height increment $d_h = 200$ m and an initial zenith wet delay of $zwd_0 = 150$ mm at all stations. Wind speeds were assumed to be 8 m s^{-1} in the eastern direction and 0 m s^{-1} towards the north. The tropospheric correlation time of the observations was set to 2 h. The clock stability was simulated with an Allan standard deviation of 1×10^{-14} at 50 min and the measurement noise was set to have a standard deviation of 15 ps.

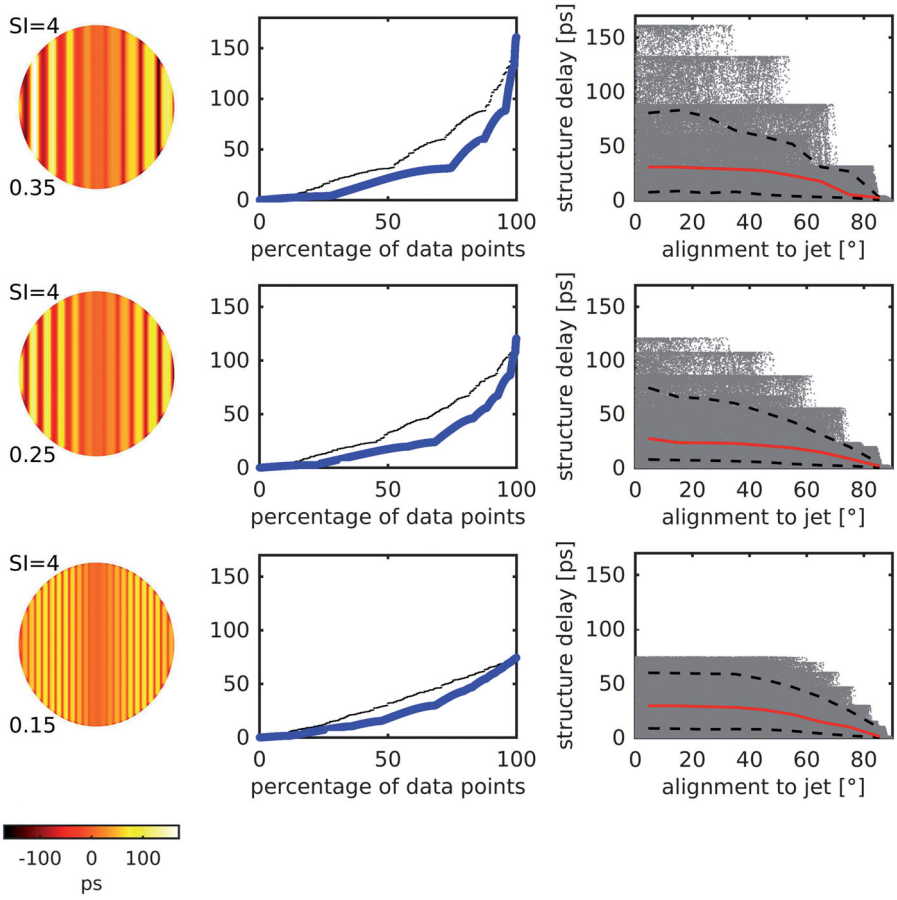

Figure 4. Same as Fig. 2, but for SI = 4.

Solving for baseline length repeatabilities, a typical measure to assess the accuracy of VLBI results, we find weighted root mean square (wrms) values of a few millimetres for the short baselines up to 2–3 cm for the longest baselines. These are realistic values for the current global VLBI results using one year of data (e.g. Plank et al. 2015). We then run three different simulations: (1) source structure-only, where the observed minus computed (O − C) values entering the least-squares adjustment were only the delays due to source structure (O − C = τ_{ss}); (2) full simulations without source structure effects, accounting for the standard geodetic stochastic error sources (O − C = $\tau_{trop} + \tau_{clk} + \tau_{wn}$); (3) full simulations (including source structure effects; O − C = $\tau_{trop} + \tau_{clk} + \tau_{wn} + \tau_{ss}$).

In total, we simulated 104 rapid sessions in which 23 stations observed 428 sources. The networks, observing schedules and observed sources vary from session to session and we fixed the positions of all sources that were observed in fewer than 20 sessions. For these 325 out of 428 sources, also no source structure delays were simulated. The other 103 sources were observed quite differently, in between 20 and 88 sessions, with 1 to 691 observations per session. Over all sessions, each source had between 34 and 12 554 observations. When applying source structure, all 103 sources were modelled with an identical two-component source model, with the direction of the jet of the source randomly varying from source to source (0°–360°).

In the analysis, we have used standard settings for the calculation of the theoretical delay (Petit & Luzum 2010). We note that all a priori information cancels in the simulation in any event. In the global solution, the source coordinates were estimated using a loose constraint (2 mas) to tie them to the a priori CRF. We chose this option rather than the commonly used no-net-rotation condition on a set of reference sources, in order to allow a proper comparison with the newly developed estimation strategy of Section 4. All other parameters such as station positions, clocks, tropospheric delays and Earth orientation parameters were estimated as arc parameters and reduced in the global solution.

3 SOURCE STRUCTURE EFFECTS ON THE CRF

In order to understand how a systematic delay due to source structure acts on estimated source positions, we performed three simulations (source structure-only, full simulations without source structure and full simulations including source structure) and determined the estimated source position offsets and their formal uncertainties in a global solution. These results are shown in Table 2. The estimated offsets in right ascension (δRA) and declination (δDec.) were combined to give a position offset on the sky d:

$$d = \sqrt{[\delta\mathrm{RA} \cdot \cos(\mathrm{Dec.})]^2 + \delta\mathrm{Dec.}^2}. \quad (3)$$

The same was done with the formal uncertainties σ_{RA} and $\sigma_{Dec.}$:

$$\sigma_d = \sqrt{[\sigma_{\mathrm{RA}} \cdot \cos(\mathrm{Dec.})]^2 + \sigma^2_{\mathrm{Dec.}}}. \quad (4)$$

Table 2. Simulated median source position offsets and formal uncertainties (see equations 3 and 4) for an estimated CRF. We compare the results of different simulations, using no source structure and structure indices of 2, 3 and 4. In the second column, the results of source structure-only simulations are shown as a median of three solutions. In the third column, we give the numbers for the full simulations, additionally including simulated errors due to clocks, troposphere and measurement noise. The full simulations were also run with three realizations.

b_r	Structure-only (μas)	Full simulations (μas)
No structure	–	49 ± 44
SI = 2.0		
0.35	25 ± 2	58 ± 44
0.30	33 ± 4	63 ± 44
0.25	63 ± 4	82 ± 45
0.20	50 ± 3	71 ± 44
0.15	35 ± 3	62 ± 44
0.10	15 ± 2	53 ± 44
0.05	7 ± 3	52 ± 44
SI = 3.0		
0.35	51 ± 9	81 ± 45
0.30	39 ± 8	72 ± 45
0.25	33 ± 8	65 ± 45
0.20	26 ± 8	57 ± 45
0.15	23 ± 9	57 ± 45
0.10	24 ± 9	56 ± 45
0.05	16 ± 9	57 ± 45
SI = 4.0		
0.35	82 ± 33	102 ± 55
0.30	60 ± 31	88 ± 54
0.25	57 ± 28	82 ± 52
0.20	47 ± 27	73 ± 52
0.15	36 ± 27	66 ± 52

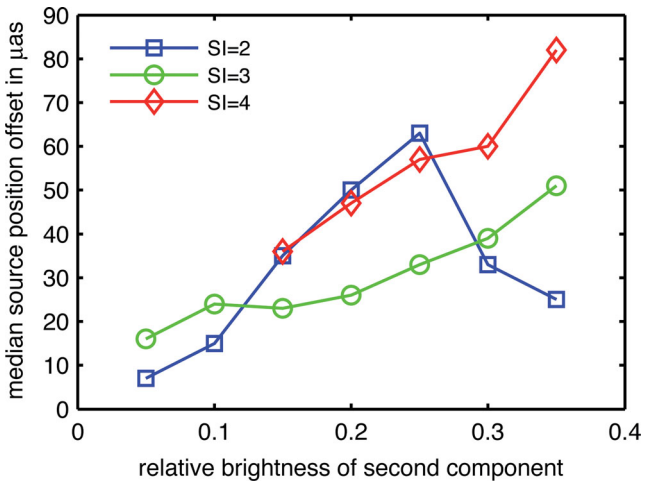

Figure 5. Simulated median source position offsets d due to source structure using various two-component source models with nominal structure indices SI = 2, 3 and 4 and a relative brightness of the second component between 0.05 and 0.35 of the main component. These are structure-only simulations.

In order to allow for a fair comparison with the results of Section 4, any correlation between σ_{RA} and $\sigma_{Dec.}$ was neglected. In the structure-only simulations, each source was assigned a random jet direction, which was then kept fixed for all source models. From the globally estimated source position offsets, the median offsets and formal uncertainties over all estimated sources are shown in Table 2 and Fig. 5.

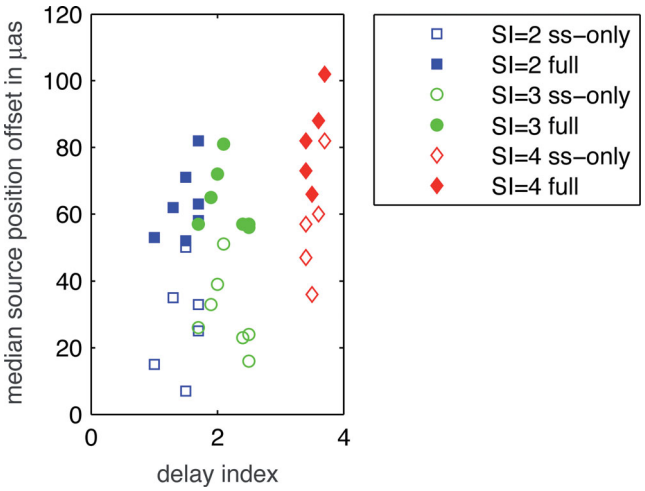

Figure 6. Simulated median source position offsets d due to source structure using various two-component source models with nominal structure indices SI = 2, 3 and 4 versus the observed delay index given in column 6 of Table 1. Both simulations are shown: source structure-only (open symbols) and full simulation (solid symbols).

We find that in the median, source structure affects the estimated source positions at the level of some tens of μas. For the simulations using sources with SI = 3 and 4, we find higher median offsets for a stronger second component (Fig. 5). This relation does not hold for the source models of nominal SI = 2. In medians, over all estimated sources, the structure of a nominal SI = 2 can cause a systematic shift of source positions at the same level (up to 60 μas) as the structure of nominal SI = 4. A clear difference between the three levels of structure indices (2, 3 and 4) is found for the formal errors. These formal errors were determined within the global solution and, to a certain extent, reflect the variation of an estimated source position offset from observation to observation and from session to session, respectively. Hence, these errors can be used as a measure of source position scatter that we would obtain in single-session solutions. As shown previously (e.g. Fey & Charlot 1997; Schaap et al. 2013), sources of higher SI show larger source position uncertainties and more scatter. The formal errors for d of 2–4 μas for SI = 2, 8–9 μas for SI = 3 and about 30 μas for SI = 4, which were found in our simulations, confirm this correlation.

It is interesting to note that the estimated source position offsets are considerably smaller than expected from the shift of the brightness centroid from the nominal core position. Despite the offset for some individual sources being as large as r_{centr} for a particular source model (see Section 3.1 and Fig. 8), in medians over all sources this nominal offset is strongly attenuated (by more than a factor of 10 for the SI = 4 models) in the analysis.

We can also compare the level of the estimated source position offsets with the observed structure delays and the corresponding delay indices SI_{obs} as given in column 6 of Table 1. This is illustrated in Fig. 6 for both simulations: source structure-only and full. Comparing the results of models with identical nominal structure indices SI = 2, 3 and 4, we find that, on average, a higher delay index appears to correlate with a higher median source position offset. However, the scatter in this correlation is evidently large. We can conclude that the delay index also, as a measure of the median structure delay of the actually observed baselines, does not necessarily correspond to a higher observed median source position offset.

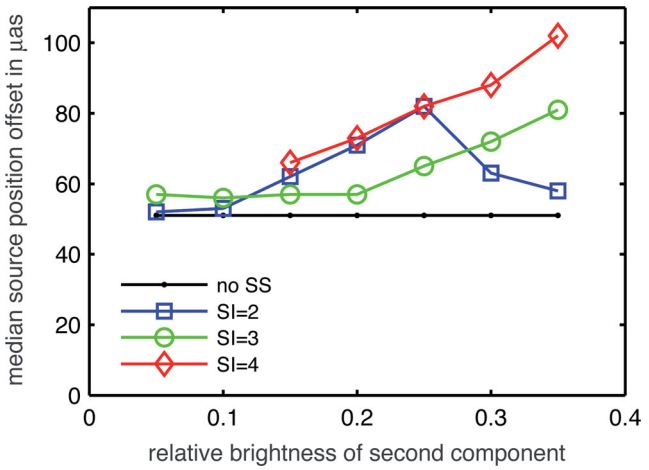

Figure 7. Simulated median position offsets d due to source structure using various two-component source models with nominal structure indices SI = 2, 3 and 4 and a relative brightness of the second component between 0.05 and 0.35 of the main component. These are full simulations, including the effects of troposphere, clock and measurement noise. The black line shows the result for the full simulations, when no source structure was simulated.

In the full simulations, we also accounted for errors due to tropospheric turbulence, station clocks and measurement noise. For control reasons, the full simulations were also repeated three times. This time, the chosen directions of the jets were kept fixed in all three repetitions, whereas new random numbers for the stochastic generation of the other error sources were used in each repetition. Without simulating source structure effects, we find median source position offsets of 49 ± 44 μas. This shows that the offsets are at roughly the same level as their formal uncertainties, a result that we expect when applying quasi-random errors. We note that the position offset d is an absolute quantity and, for the simulation without source structure, the medians of δRA and δDec. are close to zero. A comparison of the results with the nominal noise floor of the ICRF2 of 40 μas (Ma et al. 2009) again shows that our chosen parameters for the simulation give realistic results. However, it should be kept in mind that because of the time-consuming nature of simulations, we only use one year of data in our simulations.

Applying source structure, we find a significant increase in the position offsets for SI = 2, 3 and 4 (Fig. 7), but formal uncertainties are much less affected. Adding source structure of SI = 2 and 3 only increases these by 1–2 μas from the no-structure simulations, consistent with the expectations of adding the structure and the stochastic error contributions in quadrature (e.g. $\sqrt{44^2 + 3^2} = 44$ for SI = 2 and $\sqrt{44^2 + 9^2} = 45$ for SI = 3). Adding source structure of SI = 4, however, does significantly increase the formal uncertainties in our solution to 52–55 μas (as $\sqrt{44^2 + 30^2} = 53$). Even this increase, however, is insignificant compared to the effects on the estimated offset.

Our results show that although the individual effects of source structure in one session might be small compared to other error sources, its systematic behaviour causes a significant effect on the CRF, while other (stochastic) errors usually cancel over a large number of sessions. Further, the estimated offsets clearly exceed their errors.

3.1 Jet direction

So far, we have only reported median offsets over all simulated sources at the level of tens of μas. In fact, for single sources, the apparent movement in position due to source structure can be much higher, up to hundreds of μas. This is shown in Fig. 8: for each estimated source, its offset d is shown versus the alignment of this offset to the jet direction of the underlying source model. Additionally, the sources are binned in the alignment angle, and we show the median offset and the 16th and 84th percentiles for each bin.

Fig. 8 shows that the simulations yield higher source position offsets for better alignment to the jet direction. This is very clear for the first three simulations using SI = 2 source models ($b_r = 0.35$, $b_r = 0.25$ and $b_r = 0.15$) while it becomes less obvious for the SI = 3 and 4 models. We also find that most (but not all) sources are indeed moved along the jet direction of the source model. Again, this is very clear for the SI = 2 models and less so for the SI = 3 and 4 models. We present these data in Table 3, where we show the percentage of sources with estimated offsets aligned to the jet direction within less than 45°, 30° and 10°. For the SI = 2 models, with the exception of the models with $b_r = 0.10$ and $b_r = 0.05$, this alignment is generally very high: about 50 per cent of the estimated source position offsets are aligned with the jet direction to better than 10°, and almost all sources (∼90 per cent) lie within 45° of the jet. For the two models with the faintest jet components, these percentages drop to about 20–30 and 65–80 per cent for alignment within 10° and 45°, respectively.

Applying source structure models of nominal SI = 3 and SI = 4, the percentages of alignment between the estimated offsets and the jet angles are generally lower than for models of SI = 2. We find about 60–70 per cent of the estimates are aligned within 45° and about half of the estimates (40–60 per cent) within 30°. As seen in the SI = 2 simulations, the alignment appears worse for weaker, more distant secondary components. Conversely, the models of SI = 3 and 4 with a brighter, close-by secondary component cause the source positions to be shifted more along the jet direction and cause generally larger total and median offsets.

Figs 2, 5 and 8 and Table 2 allow us to draw some more conclusions about the variability in the effects of different source structure models of SI = 2. Almost no effects on the source positions (7 and 15 μas in medians, respectively) are found for the models of $b_r = 0.10$ and $b_r = 0.05$. The median values are close to the maximal source position offsets for single sources, which is about 30 μas for a relative brightness of $b_r = 0.05$ (Fig. 8, top right). An explanation for the minor effect is found in the bottom row of Fig. 2: at moderate beating of the delay amongst all baseline lengths, a maximum delay of about 15 ps is found, with 84 per cent of all structure delays being smaller than 8 ps. In contrast, when the secondary component is stronger ($b_r = 0.35$, top row) the distribution of the structure delay in the (u, v) plane shows almost no beating at all. We find predominantly very low structure delays (84 per cent below 5 ps) and some extremely high delays of up to 20 ps for some long baselines aligned to the jet. These few but high structure delays have a significant effect on some of the sources, displacing them by up to 50–60 μas (Fig. 8, top left). This displacement is well aligned with the direction of the jet. For the other SI = 2 models, it becomes clear that while the median delays do not change much, the differences are found in the distribution of the second half of all delays, as indicated by the line for the 84th percentile (Fig. 2, right column). Because this effect is systematic, estimated source positions are preferentially shifted in the direction of the jet, by up to 50–100 μas for many sources when applying source structure of SI = 2 ($b_r = 0.25$ and $b_r = 0.15$). Consequently, we also find higher median source position offsets for these models in Table 2.

For the SI = 3 models, the smallest effect on source position offsets is also found for the weakest and most distant secondary

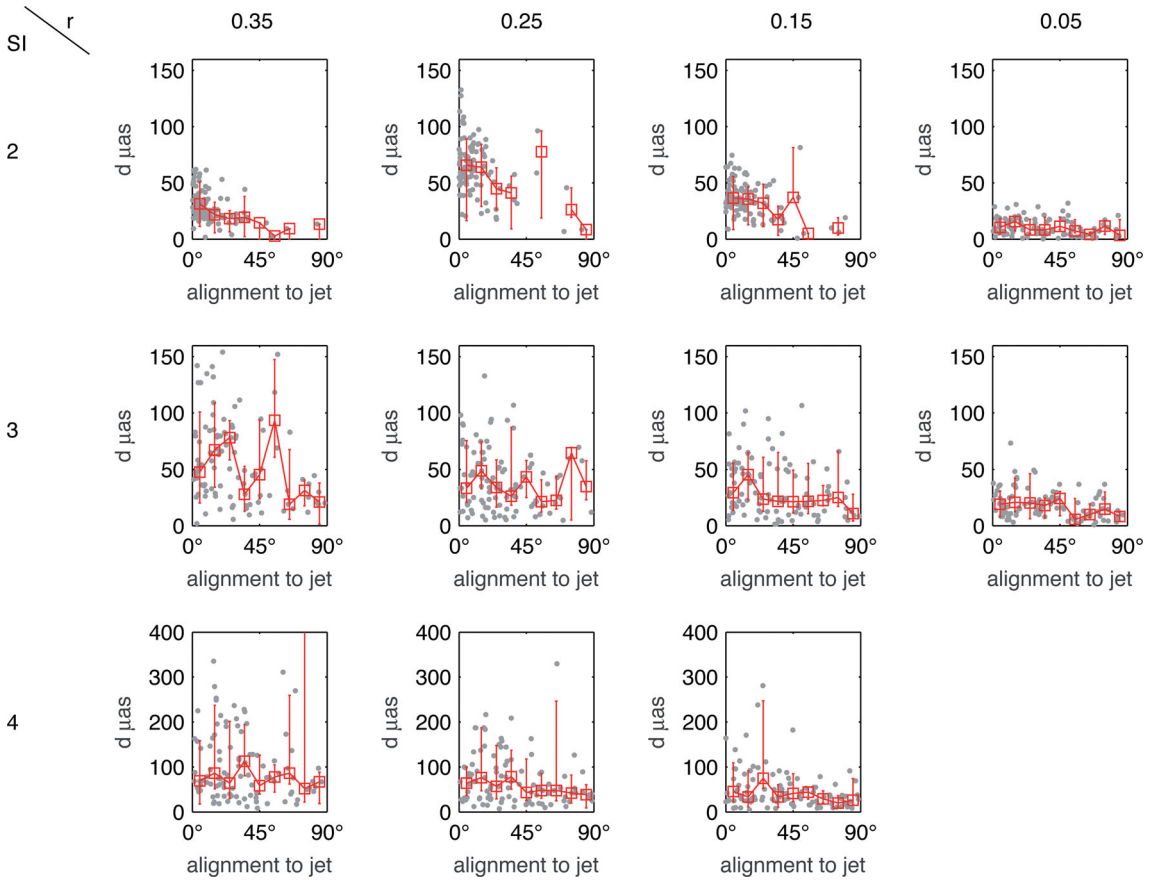

Figure 8. Estimated position offsets d due to simulated source structure per source using various structure models with a nominal structure index SI = 2 (top), SI = 3 (middle) and SI = 4 (bottom). The x-axis shows the alignment [0–90°] of the direction of the estimated offset with the direction of the source's jet. Additionally, the estimated offsets are binned by alignment with the jet in increments of 10°, with the red squares and whiskers indicating the median source position offset as well as the 16th and the 84th percentile for each bin. Note the different scaling for different structure indices.

component ($b_r = 0.05$), affecting source positions up to only about 30 µas at most. With increasing brightness of the secondary component, the beating of patterns in structure delay in the (u, v) plane decreases and the areas of similar structure delay become broader. While the median delays of all observations do not change significantly, the maximal delays as well as the distribution of the upper 16–50 per cent of structure delays change noticeably. For a relative brightness $b_r = 0.35$, source positions are moved by up to 100–150 µas (51 µas in median), values more typical for the SI = 4 models. In contrast to applying source structure of SI = 2, the SI = 3 models also affect a number of sources, which are moved into directions other than parallel to the jet. For sources with extremely large estimated offsets, we searched for anomalies in the observing schedules (low number of observations, low number of sessions, etc), without any success. As a reminder, we note here that identical schedules were used for all investigations, meaning that any differences between applying different source structure models are the results of the particular combination of that model with the given geometry as defined in the schedules we used.

The biggest difference between the SI = 4 models is in the maximum structure delays, which coincides well with an increase in both maximal and median source position offsets. We can conclude that for the SI = 4 models, the beating in the (u, v) plane is generally high and hence the interplay between a particular pattern with the observational geometry becomes less important. In other words, the effect of this highest level of structure produces delays that are less consistent with a source position offset in the direction of the jet and, although greater in magnitude, tend to be relatively reduced in a global solution over all sessions.

Summarizing this section, we find that source structure causes an apparent shift of the source position, which is mostly but not always aligned with the direction of the jet of that source. Because the observing geometry of the simulations did not change, the reason for the alignment/non-alignment of the estimated source offsets lies in the different source structure models. Systematic source offsets are also found in the full simulations. Despite other (largely stochastic) simulated errors causing an additional shift in positions, the systematic effect due to structure remains. Hence, when the estimated source position offsets of the full simulations are reduced by the results of the full simulations without additional source structure, the results are identical with those of the structure-only simulations. This is a cross-check of our simulations.

4 NEW PARAMETRIZATION

In this section, a new parametrization is tested with the goal of mitigating the effects of source structure on a globally estimated CRF. In Section 3.1, we have shown that source structure leads to position offsets preferentially in the jet direction. Motivated by this, the idea is to represent source positions in components along the jet (j) and perpendicular to the jet (normal component, n), rather than the usual RA/Dec. parametrization. The j-component is then

Table 3. Alignment of the estimated position offsets with the jet direction of the sources. The percentages of all sources are shown, where the offset is aligned within 45°, 30° and 10°, respectively. This is given for source structure-only simulations using the various models of nominal structure indices 2, 3 and 4. The values are medians of three solutions, each time using different jet directions for each source.

b_r	<45° (per cent)	<30° (per cent)	<10° (per cent)
SI = 2.0			
0.35	95	90	56
0.30	88	78	43
0.25	96	92	61
0.20	96	92	59
0.15	93	87	50
0.10	81	64	29
0.05	65	46	23
SI = 3.0			
0.35	77	64	29
0.30	76	63	25
0.25	75	58	22
0.20	73	58	28
0.15	66	50	22
0.10	74	54	17
0.05	69	52	20
SI = 4.0			
0.35	73	53	19
0.30	68	53	18
0.25	66	50	20
0.20	66	47	18
0.15	60	41	18

modelled as an arc parameter and session-wise reduced. In the global solution, only the component normal to the jet direction contributes to the final CRF.

Such a set-up in the analysis is also supported astrophysically because, although the actual structure of a source is subject to change considerably with time, the direction of the jet is generally thought to remain constant (e.g. Lister et al. 2009). Studying the variation of the jet direction in images of 44 frequently observed geodetic sources, we have found that for 30 per cent of the sources the jet angle is stable within 5°, and within 10° for 65 per cent of the studied sources. The investigated time-span was up to 17 yr and we had between a minimum of 2 and a maximum of 22 images per source (median = 5).

4.1 Formalism

Unlike the usual barycentric source coordinates in RA and Dec., the j/n parametrization is different for each source. The source catalogues of the VieVS source structure simulator contain only two component sources (Section 2.1). The direction of the jet ($\boldsymbol{j}$) is given by the line between these two components, the normalized offset in right ascension and declination (ΔRA and ΔDec.), respectively. The vector perpendicular to the jet direction ($\boldsymbol{n}$), as seen in the RA/Dec. plane on the sky, can be directly derived by interchanging the two components of the vector and changing the sign for one of the components (equation 5):

$$\boldsymbol{j} = \begin{pmatrix} \Delta\mathrm{RA} \\ \Delta\mathrm{Dec.} \end{pmatrix}, \boldsymbol{n} = \begin{pmatrix} \Delta\mathrm{Dec.} \\ -\Delta\mathrm{RA} \end{pmatrix}. \quad (5)$$

Table 4. Simulated median source position offsets d and formal uncertainties for an estimated CRF using the new j/n parametrization. We compare the results of different simulations, using no source structure and source models of nominal structure indices of SI = 2, 3 and 4. The presented values are medians for three realizations of each simulation, with new jet angles for the structure-only simulations and new random numbers for the stochastic errors sources in the full simulations respectively.

b_r	Structure-only (μas)	Full simulations (μas)
No structure	–	38 ± 44
SI = 2.0		
0.35	4 ± 2	38 ± 41
0.30	6 ± 3	39 ± 41
0.25	8 ± 4	41 ± 41
0.20	7 ± 3	40 ± 41
0.15	6 ± 2	39 ± 41
0.10	4 ± 2	39 ± 41
0.05	4 ± 3	39 ± 41
SI = 3.0		
0.35	16 ± 8	44 ± 41
0.30	14 ± 7	42 ± 41
0.25	11 ± 7	41 ± 41
0.20	9 ± 7	39 ± 41
0.15	11 ± 8	40 ± 41
0.10	10 ± 8	38 ± 41
0.05	8 ± 8	38 ± 41
SI = 4.0		
0.35	39 ± 30	63 ± 51
0.30	30 ± 28	55 ± 50
0.25	27 ± 25	49 ± 48
0.20	28 ± 24	54 ± 48
0.15	22 ± 24	48 ± 47

For the new parametrization, the partial derivatives of the observable τ with respect to the source position ($\boldsymbol{j}$, $\boldsymbol{n}$) were set up as follows:

$$\frac{\partial\tau}{\partial\boldsymbol{j}} = \frac{\partial\tau}{\partial\mathrm{RA}}\Delta\mathrm{RA} + \frac{\partial\tau}{\partial\mathrm{Dec.}}\Delta\mathrm{Dec.}$$
$$\frac{\partial\tau}{\partial\boldsymbol{n}} = \frac{\partial\tau}{\partial\mathrm{RA}}\Delta\mathrm{Dec.} - \frac{\partial\tau}{\partial\mathrm{Dec.}}\Delta\mathrm{RA}. \quad (6)$$

In the global solution, the normal equation matrices of all 104 sessions were stacked together. While the parallel component was reduced session-wise (meaning that the source was allowed to move along the jet in each session), only the normal component was set up as a global parameter using loose constraints of 2 mas for all estimated sources. As a result, we obtain an estimated position offset in the normal direction n, as well as its formal uncertainty σ_n. Finally, the estimated values for the n-component could be transformed to corrections in RA and Dec. using equation (5), and subsequently into a position offset on the sky d according to equation (3).

4.2 Results

The new parametrization was applied to all the simulations described in Section 3. The results in terms of median source position offsets and uncertainties using the new parametrization are given in Table 4 and Figs 9 and 10.

When applying the new j/n parametrization, we find that the distorting effect on an estimated CRF is diminished. A careful examination of the findings is in order. In the full simulation without source structure, the median estimated source position offset is

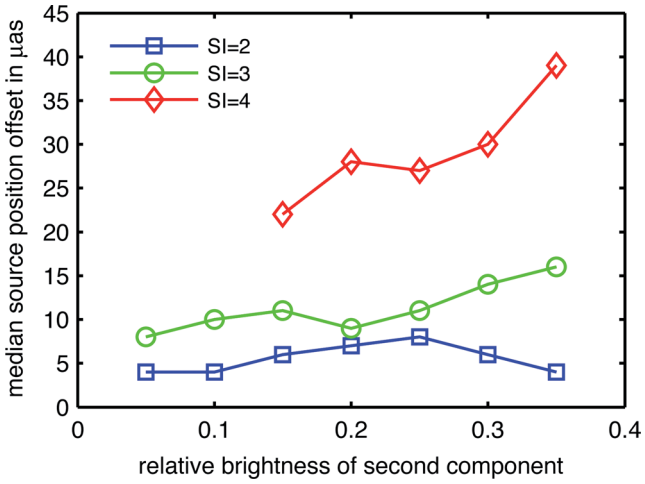

Figure 9. Simulated median position offsets d due to source structure using various two-component source models with nominal structure indices SI = 2, 3 and 4 and a relative brightness of the second component between 0.05 and 0.35 of the main component. These are structure-only simulations using the new j/n parametrization.

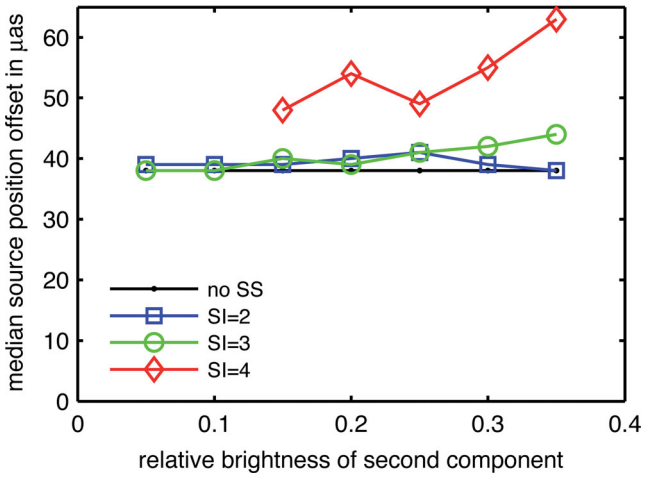

Figure 10. Same as Fig. 9 but for full simulations. The black line shows the result for the full simulation, when no source structure was simulated.

reduced from 49 μas (Table 2) to 38 μas (Table 4), while the formal errors with 44 μas stay the same. This slight reduction is due to the fact that in the new parametrization we allow the source to move along one direction per session. Hence, the free coordinate effectively absorbs some of the stochastic errors.

Applying source structure of SI = 2, the new method is found very suitable. From originally up to 60 μas in median systematic source position offsets, we could reduce the effect to a level below 10 μas. For SI = 3, the median offsets could be reduced from about 20–50 μas to the level of 8–16 μas. A slight increase in the estimated source position offset for a stronger secondary component is still evident in Figs 9 and 10. For SI = 4, although the median offsets are more or less halved (from 40–80 μas to 20–40 μas) when applying the new parametrization, the effects of source structure on global source positions are still clearly evident. The formal uncertainties remain about the same for the new method as for the classical method.

The full simulations let us better assess the significance of the remaining median systematic offsets. Fig. 10 shows that for the structure of a nominal SI = 2 and 3, the overall level of remaining offsets is only slightly (<10 μas) above the solution without source structure. This is not the case for the SI = 4 structure where, despite the new j/n parametrization, applying source structure significantly moves the sources.

More insight into the functionality of the new estimation procedure is given through Fig. 11. As in Fig. 8, the median source position offsets are given for bins of alignment, comparing the classical parametrization with the new j/n approach.

It is clearly visible that the estimated offsets that were well aligned to the jet direction are heavily diminished while the estimates in other directions are less affected. As in the SI = 2 simulations, most estimated offsets are aligned with the jet (up to 90 per cent within 30–40°; see Table 3), and the new parametrization proves to be very suitable for mitigating the effects of source structure at the level of SI = 2 on the CRF. For SI = 3, the alignment was less good and hence the success of the new parametrization is limited. We find a satisfying mitigation up to an alignment of the estimated sources of 30–40°, which, according to Table 3, means for at least 50 per cent of all sources.

Care has to be taken when the new method is applied for reducing the effects of simulated structure of SI = 4. While the offsets due to source structure along the direction of the jet are greatly suppressed when applying the new parametrization, offsets initially estimated in the normal direction are found to remain at the level of up to about 50 μas (medians) for some models (Fig. 11).

However, once again we find differences between the different source models. Hence, for models of SI = 4 with a weaker secondary component (b_r = 0.15, 0.20 and 0.25) further away, the new parametrization greatly suppresses source position displacements due to structure (to a level of about 30 μas) when the estimated offset is aligned with the direction of the jet within 45°. Conversely, for models with a close and strong second component (b_r = 0.30 and 0.35), high (30–50 μas) median source position offsets are also found for well-aligned estimated offsets 30–45°. This is also reflected in overall higher median source position offsets over all sources for these models (Table 4).

The above results are motivating, but also show some limitations of this new approach. We clearly see that the influence of source structure is better mitigated for better alignment. In general, the new approach greatly reduces the effects of source structure for good alignment (about up to 30–40°) between the jet angle and estimated source position offset, while the improvements are less clear for sources whose estimated offsets are less aligned with the direction of the jet.

5 DISCUSSION

The presented simulations show that the source structure of SI = 2 and above can systematically affect source positions at a level above the ICRF2 noise floor and above the influence of the most common stochastic error sources, tropospheric turbulence, clock errors and measurement noise. This is particularly interesting because the current limit for the selection of suitable radio sources is SI < 3.0 (Ma et al. 2009). The effects found in our simulations are solely the result of observing different sessions with different baselines and changing networks. Other effects, such as the variation of source structure with time or the apparent change in the core position with frequency (e.g. Lobanov 1998; Charlot 2002; Kovalev et al. 2008), were not included in this study.

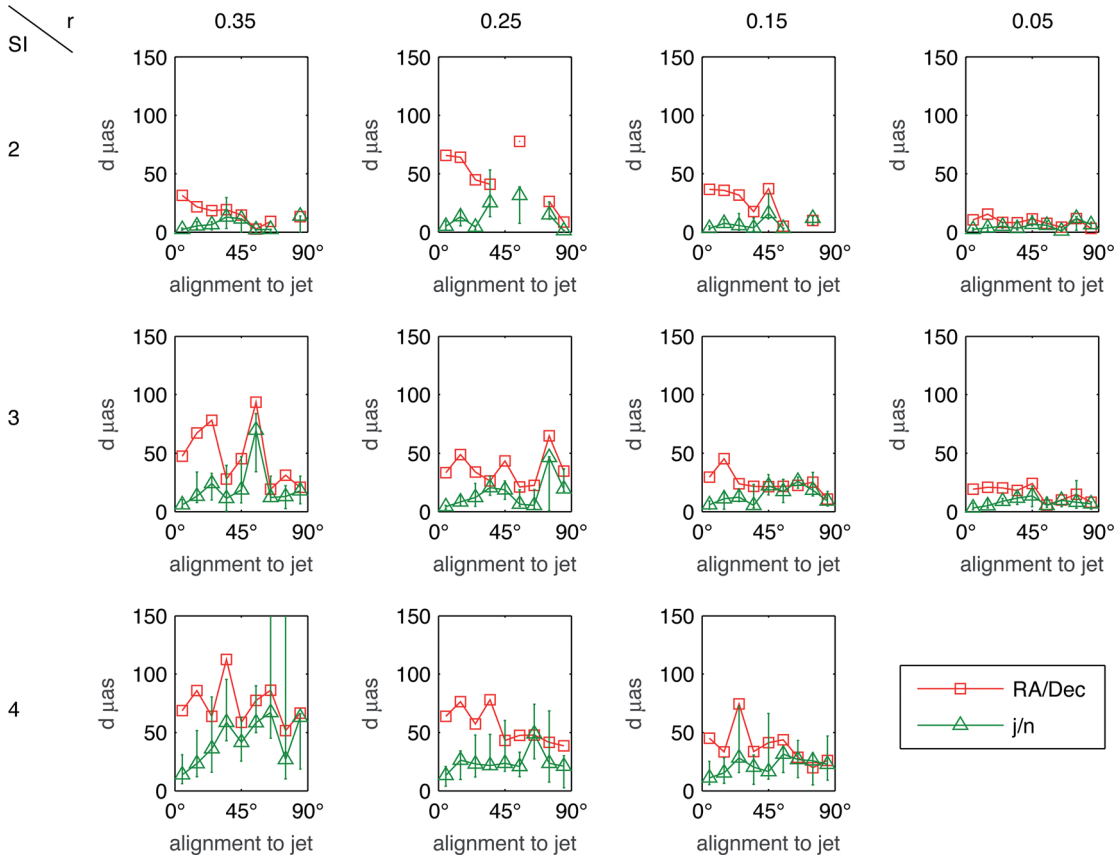

Figure 11. Comparison of the simulated position offsets d due to source structure between the estimates of the classical RA/Dec. solution and the new j/n parametrization for source structure-only simulations. Results are given for various structure models, with a nominal structure index SI = 2 (top), SI = 3 (middle) and SI = 4 (bottom). The x-axis shows the alignment [0–90°] of the direction of the estimated offset with the direction of the source's jet. The estimated offsets of the individual sources are binned by alignment with the jet in increments of 10°, with the green triangles (red squares) and whiskers indicating the median source position offset as well as the 16th and the 84th percentiles for each bin. For a better comparison also between the different levels of structure indices, a common scaling is used in all plots.

By applying different two-component source models, we have also found large differences in the size and the characteristics of the estimated source position offsets, even when their nominal structure indices were identical. These clear differences between the models are a result of the clear beating pattern in the (u, v) plane: source structure models with low SI, which are not frequently beating, show a strong systematic effect on global source positions, although their individual structure delays are quite small. Conversely, the effects of SI = 4, showing a high variability of the structure delay in the (u, v) plane, are individually much larger but tend to become absorbed in the large sample of observations, baselines and sessions. Although many real radio sources are reducible to a two-component model (Charlot 1990), this could change considerably when additional components are added to the source model. This needs to be investigated in the future, for example by using real source models from imaging data.

We have further found that, although the observed delay index SI_{obs} might better reflect the actual structure delays in a specific network and observation set-up than the network independent nominal SI, it is also not suitable as a proper indicator for the size of the effect on the CRF.

The presented simulations confirm the work by Moór et al. (2009), who, using real observations, also found that the correlation between observed source movement and jet direction does not hold for all sources. As pointed out by MacMillan & Ma (2007), variations in source positions can also occur due to changes in the observing antenna network. This was clearly shown here. While further research will be necessary for a full understanding of the interactions between the observing network, the schedule, the behaviour of source structure and the resulting source position offset, we have shown that slight changes in the source model (keeping the nominal SI fixed) can significantly change the estimated source position, even for a fixed observing geometry.

The newly presented parametrization using the direction of the jet was found to be effective at reducing the apparent effects on a globally estimated CRF. The improvement is greater for sources whose position offset was actually found to be well aligned with the direction of the jet using a standard parametrization. In our case study, this means that this method is more suitable for sources with structure indices SI = 2 and SI = 3 rather than SI = 4. We note that this might also be a limitation of the applied simulation method.

The used source models consisting of two components only were rather simple and stable with time. In reality, we expect a dynamic source evolution with multiple components moving predominantly along the jet. This needs to be investigated in the future. However, we have examined a large number of source models, applying a range of astrophysically reasonable separations and brightness ratios between the modelled source components. Further testing, especially with real source models from imaging (not two-component models), will be necessary.

Our new parametrization strategy should be used with discretion. One does not want to lose valuable position information on good and stable sources by modelling one direction as an arc-parameter. A better approach might be to apply the traditional analysis for all stable sources, and to model the unstable sources with the new j/n parametrization. We defer this approach to a future investigation.

6 CONCLUSIONS

We have used the source structure simulator of VieVS to simulate the effects of source structure delays on globally estimated source positions. Our findings confirm previous studies with real observations that source structure can affect the CRF at the level of tens to hundreds of mas for individual sources. These effects are evident for source models that are not changing with time. Because of its systematic behaviour, in the global solution this effect exceeds other common error sources due to the station clocks, tropospheric turbulence or measurement noise, which are individually larger but usually cancel in a larger sample of observed sessions.

Applying simple two-component models for the observed sources, we find that in medians over all sources, the size of the offsets does not necessarily scale with increasing SI. We find that sources of nominal structure indices of SI = 2, 3 and 4 can all cause offsets above the current level of source position uncertainties. Here, the determined offset in source position is the result of the additional delay due to source structure applied in one year of geodetic schedules, and the subsequent determination of a CRF in a global solution. Another interesting result is the fact that most source models of a lower structure index (SI = 2) cause source position offsets more or less ($<30^\circ$) aligned with the jet direction of the underlying source model. Despite almost all simulated models showing an alignment within 30° for at least 50 per cent of the estimated sources, this clear relation significantly weakens for higher structure indices. The reason for this could be identified as the more dense beating pattern of the structure delay as seen in the (u, v) plane, causing high structure delays even for relatively unaligned baselines. Another important finding of this simulation study is the fact that the effects of source structure due to simple two-component models on an estimated CRF can significantly vary for slightly different models, even when the nominal SI of these models is the same.

Finally, we have presented a new parametrization, where the source positions are modelled in components along the jet and perpendicular to it. In the global solution, the component perpendicular to the jet is assumed to be stable and contributes to the CRF estimations, while the component along the jet is modelled as an arc-parameter and is reduced session-wise. Applying this new parametrization significantly reduces the negative effects due to source structure, for certain models even down to the level of the formal uncertainties. The study also reveals some problematic issues for such a new modelling approach, especially when the underlying source structure does not necessarily cause the sources to be shifted along the jet direction, which is often the case for the SI = 4 models.

Negative effects of source structure in *X*-band VLBI have long been identified to be problematic in geodetic and astrometric VLBI and specifically in defining a stable celestial reference frame. Because of its complexity as well as the fact that sources change with time, no fully satisfactory mitigation strategy has yet been found. At present, sources having a high SI or revealing considerable instabilities in their position time series are excluded from the set of ICRF defining sources. In this study, we have shown that for most (but not all) of the source models of SI < 3 the systematic errors due to source structure are smaller (a few tens of μas) than the errors due to the troposphere or than the overall nominal noise level of the ICRF (40 μas). According to this, the current restriction to sources of SI < 3 is a semisuccessful mitigation strategy. However, for more stringent accuracy demands, source structure effects will become more problematic. Our newly presented parametrization modelling with respect to the jet direction could provide a potential solution for this problem. It successfully suppresses source structure effects down to the level of below 10 μas for SI = 2 and SI = 3 sources. Applying the j/n parametrization to sources currently classified as unstable might allow these to contribute to the ICRF datum by providing a stable position at least in one direction.

Another possibility for mitigation of the source structure-induced errors in a CRF would be to move it to higher frequencies, for example X/KA-bands (8.4/32 GHz) as proposed by Jacobs et al. (2012). Sources at these higher frequencies are thought to be more compact and to have less intrinsic structure, resulting in an improved CRF (Charlot et al. 2010). A detailed study of source structure effects at higher frequencies will be the subject of future research.

ACKNOWLEDGEMENTS

The authors would like to thank the IVS and all its components for their continuous efforts in the coordination of global VLBI measurements. We used images of the Astrogeo Center Data base of Brightness Distributions, Correlated Flux Densities, and Images of Compact Radio Sources Produced with VLBI to validate our source models. This work was supported by the AuScope Initiative, funded under the National Collaborative Research Infrastructure Strategy (NCRIS), an Australian Commonwealth Government Programme. LP, JM and SS would like to thank the Australian Research Council for Fellowships FS1000100037, FS110200045 and DE130101399. HK works within the Hertha Firnberg position T 697-N29, funded by the Austrian Science Fund (FWF). We would like to thank Chris Jacobs for his valuable comments as a referee and we also acknowledge Jonathan Rogers for his careful work on jet angles.

REFERENCES

Böhm J., Böhm S., Nilsson T., Pany A., Plank L., Spicakova H., Teke K., Schuh H., 2012, in Proc. 2009 International Association of Geodesy (IAG) Symposium, Vol. 136.

Bouffet R., Charlot P., Lambert S., 2013, in Zubko N., Poutanen M., eds, Proc. 21st Meeting of the European VLBI Group for Geodesy and Astrometry. p. 39

Charlot P., 1990, AJ, 99, 1309

Charlot P., 1993, in Campbell J., Nothnagel A., eds, Proc. 9th Working Meeting on European VLBI for Geodesy and Astrometry. Mitteilungen aus den Geodätischen Instituten der Rheinischen Friedrich-Wilhelms-Universität Bonn, p. 171

Charlot P., 2002, in Vandenberg N., Baver K., eds, International VLBI Service for Geodesy and Astrometry 2002 General Meeting Proceedings. NASA Goddard Space Flight Center, Greenbelt, MD, p. 233

Charlot P. et al., 2010, AJ, 139, 1713

Cohen M. H., Cannon W., Purcell G. H., Shaffer D. B., Broderick J. J., Kellermann K. I., Jauncey D. L., 1971, ApJ, 170, 207

Fey A., Charlot P., 1997, ApJ, 111, 95

Homan D. C., 2012, Int. J. Mod. Phys.: Conf. Ser., 8, 163

Jacobs C. S., Clark J. E., García-Miró C., Horiuchi S., Romero-Wolf A., Snedeker L., Sotuela I., 2012, in 23rd International Symposium on Space Flight Dynamics.

Knight C. A., Robertson D. S., Shapiro I. I., Whitney A. R., Clark T. A., Goldstein R. M., Marandino G. E., Vandenberg N. R., 1971, Sci, 172(3978), 52-4
Kovalev Y.Y, Lobanov A. P., Pushkarev A. B., Zensus J. A., 2008, A&A, 483, 759
Krásná H., Böhm J., Plank L., Nilsson T., Schuh H., 2014, in Rizos C., Willis P., eds, Proc. IAG Symp. 139, Earth on the Edge: Science for a Sustainable Planet. Springer, Berlin, p. 203
Lindegren L. et al., 2008, in Jin W. J., Platais I., Perryman M. A. C., eds, Proc. IAU Symp. 248, A Giant Step: from Milli- to Micro-arcsecond Astrometry. Kluwer, Dordrecht, p. 217
Lister M. et al., 2009, AJ, 138, 1874
Lister M. et al., 2013, AJ, 146, 120
Lobanov A. P., 1998, A&A, 330, 79
Ma C. et al., 1998, AJ, 116, 516
Ma C. et al., 2009, in Fey A., Gordon D., Jacobs C.S., eds, IERS Technical Note 35, Verlag des Bundesamts für Kartographie und Geodäsie, Frankfurt am Main
MacMillan D., Ma C., 2007, J. Geod., 81, 443
Moór A., Frey S., Lambert S., Titov O., Bakos J., 2009, AJ, 141, 178
Nilsson T., Haas R., Elgered G., 2007, in Böhm J., Pany A., Schuh H., eds, Proc. 18th European VLBI for Geodesy and Astrometry Working Meeting, Vol. 79. p. 175
Pany A., Böhm J., MacMillan D. S., Schuh H., Nilsson T., Wresnik J., 2011, J. Geod., 85, 39
Petit G., Luzum B., eds, 2010, IERS Conventions 2010. Verlag des Bundesamtes für Kartographie und Geodäsie, Frankfurt am Main
Petrachenko B. et al., 2009, NASA/TM-2009-214180
Piner B. G., Mahmud M., Fey A. L., Gospodinova K., 2007, AJ, 133, 2357
Plank L., Lovell J., Böhm J., Shabala S., Titov O., 2015, Adv. Space Res., 56, 204
Porcas R., 2009, A&A, 505, L1
Porcas R., 2010, in Behrend D., Baver K., eds, International VLBI Service for Geodesy and Astrometry 2010 General Meeting Proceedings. NASA Goddard Space Flight Center, Greenbelt, MD, p. 8
Ros E., 2012, in Ojha R., Thompson D., Dermer C., eds, Fermi and Jansky: Our Evolving Understanding of AGN, eConf C1111101.
Schaap R., Shabala S., Ellingsen S., Titov O., Lovell J., 2013, MNRAS, 434, 585
Schuh H., Behrend D., 2012, J. Geodyn., 61, 68
Schuh H., Böhm J., 2013, in Xu G., ed., Sciences of Geodesy – II. Springer, Berlin, p. 339.
Shabala S., Rogers J. G., McCallum J. N., Titov O. A., Blanchard J., Lovell J. E. J., Watson C. S., 2014, J. Geod., 88, 575
Shabala S., McCallum J., Plank L., Böhm J., 2015, J. Geod., 89, 873
Sovers O. J., Fanselow J. L., Jacobs C. S., 1998, Rev. Mod. Phys., 70, 1393
Sovers O., Charlot P., Fey A., Gordon D., 2002, in Vandenberg N., Baver K., eds, International VLBI Service for Geodesy and Astrometry 2002 General Meeting Proceedings, NASA/CP-2002-210002. NASA Goddard Space Flight Center, Greenbelt, MD, p. 243
Tornatore V., Charlot P., 2007, J. Geod., 81, 469
Whitney A. R. et al., 1971, Sci, 173, 225

This paper has been typeset from a TEX/LATEX file prepared by the author.